THE JOURNAL OF BIOLOGICAL CHEMISTRY VOL. 283, NO. 45, pp. 31097–31106, November 7, 2008

Diverse Functional Consequences of Mutations in the Na^+/K^+-ATPase α_2-Subunit Causing Familial Hemiplegic Migraine Type 2*

Received for publication, April 10, 2008, and in revised form, July 18, 2008 Published, JBC Papers in Press, August 26, 2008, DOI 10.1074/jbc.M802771200

Neslihan N. Tavraz[‡1], Thomas Friedrich[‡1,2], Katharina L. Dürr[‡], Jan B. Koenderink[§], Ernst Bamberg[¶], Tobias Freilinger[‖], and Martin Dichgans[‖]

From the [‡]Technical University of Berlin, Institute of Chemistry, D-10623 Berlin, Germany, the [§]Radboud University Nijmegen Medical Centre, Department of Pharmacology and Toxicology, Nijmegen Centre for Molecular Life Sciences, NL-6500 HB Nijmegen, The Netherlands, the [¶]Max-Planck-Institute of Biophysics, Department of Biophysical Chemistry, D-60438 Frankfurt am Main, Germany, and the [‖]Ludwig-Maximilians-Universität München, Neurologische Klinik, Klinikum Großhadern, D-81377 München, Germany

Mutations in *ATP1A2*, the gene coding for the Na^+/K^+-ATPase α_2-subunit, are associated with both familial hemiplegic migraine and sporadic cases of hemiplegic migraine. In this study, we examined the functional properties of 11 *ATP1A2* mutations associated with familial or sporadic hemiplegic migraine, including missense mutations (T263M, T376M, R383H, A606T, R763H, M829R, R834Q, R937P, and *X*1021R), a deletion mutant (del(K935-S940)ins(I)), and a frameshift mutation (S966fs). According to the Na^+/K^+-ATPase crystal structure, a subset of the mutated residues (Ala^{606}, Arg^{763}, Met^{829}, and Arg^{834}) is involved in important interdomain H-bond networks, and the C terminus of the enzyme, which is elongated by the *X*1021R mutation, has been implicated in voltage dependence and formation of a third Na^+-binding site. Upon heterologous expression in *Xenopus* oocytes, the analysis of electrogenic transport properties, Rb^+ uptake, and protein expression revealed pronounced and markedly diverse functional alterations in all ATP1A2 mutants. Abnormalities included a complete loss of function (T376M), impaired plasma membrane expression (del(K935-S940)ins(I) and S966fs), and altered apparent affinities for extracellular cations or reduced enzyme turnover (R383H, A606T, R763H, R834Q, and *X*1021R). In addition, changes in the voltage dependence of pump currents and the increased rate constants of the voltage jump-induced redistribution between E_1P and E_2P states were observed. Thus, mutations that disrupt distinct interdomain H-bond patterns can cause abnormal conformational flexibility and exert long range consequences on apparent cation affinities or voltage dependence. Of interest, the *X*1021R mutation severely impaired voltage dependence and kinetics of Na^+-translocating partial reactions, corroborating the critical role of the C terminus of Na^+/K^+-ATPase in these processes.

Familial hemiplegic migraine (FHM)[3] is a rare autosomal dominant variant of migraine with aura. It is clinically characterized by the presence of transient motor weakness in addition to other cortical symptoms as part of the migraine aura. FHM has been associated with mutations in three different genes. The *CACNA1A* gene (FHM1) (1, 2) and *SCN1A* gene (FHM3) (3, 4) both encode neuronal voltage-gated ion channels, whereas the *ATP1A2* gene (FHM2) encodes the α_2-subunit of the Na^+/K^+-ATPase (5). These observations suggest a key role for cation translocation in the pathophysiology of FHM and possibly in migraine in general (6).

The Na^+/K^+-ATPase utilizes the free energy of ATP hydrolysis to export three Na^+ ions and import two K^+ ions per ATP molecule according to the Post-Albers scheme (Fig. 1*A*) (7, 8). It generates net current and maintains the transmembrane gradients of Na^+ and K^+ (9, 10), which are critical for numerous secondary active transporters or ion channels. Functional Na^+/K^+-ATPase consists of a large catalytic α-subunit and a smaller accessory β-subunit. Both subunit isoforms are expressed in a tissue-specific and developmentally specific manner (11). In the adult brain, the α_2-subunit is mainly located in glial cells (12–15).

To date, 33 different alleles of *ATP1A2* have been associated with FHM, and nine have been associated with SHM (5, 16–27). Only five of them have been functionally examined. L764P and W887R led to nonfunctional proteins (5, 28), whereas others resulted in partially active enzymes with decreased (T345M) or increased (R689Q and M731T) K^+ affinities or reduced turnover rates (R689Q and M731T) (29, 30). These findings suggested that broad experimental approaches are required to cover the diversity of functional disruptions caused by FHM2 mutations.

In this study we analyzed a set of 11 *ATP1A2* alleles associated with familial or sporadic hemiplegic migraine. All of the

* This work was supported by the Max-Planck-Gesellschaft and Deutsche Forschungsgemeinschaft Grants (DI 722/8-2, KFG K1 027, KFG K1 028, and SFB 740 TPC4, Cluster of Excellence "Unifying Concepts in Catalysis"). The costs of publication of this article were defrayed in part by the payment of page charges. This article must therefore be hereby marked "*advertisement*" in accordance with 18 U.S.C. Section 1734 solely to indicate this fact.

[1] These authors contributed equally to this work.

[2] To whom correspondence should be addressed: Technical University of Berlin, Institute of Chemistry Sekr. PC-14, Strasse des 17 Juni 135, D-10623 Berlin, Germany. Tel.: 49-30-31424128; Fax: 49-30-31478600; E-mail: friedrich@chem.tu-berlin.de.

[3] The abbreviations used are: FHM, familial hemiplegic migraine; SHM, sporadic hemiplegic migraine; WT, wild type; SERCA, sarcoendoplasmatic reticulum Ca^{2+}-ATPase; CSD, cortical spreading depression; MOPS, 3-(*N*-morpholino)-propanesulfonic acid; MES, 2-(*N*-morpholino)-ethanesulfonic acid.

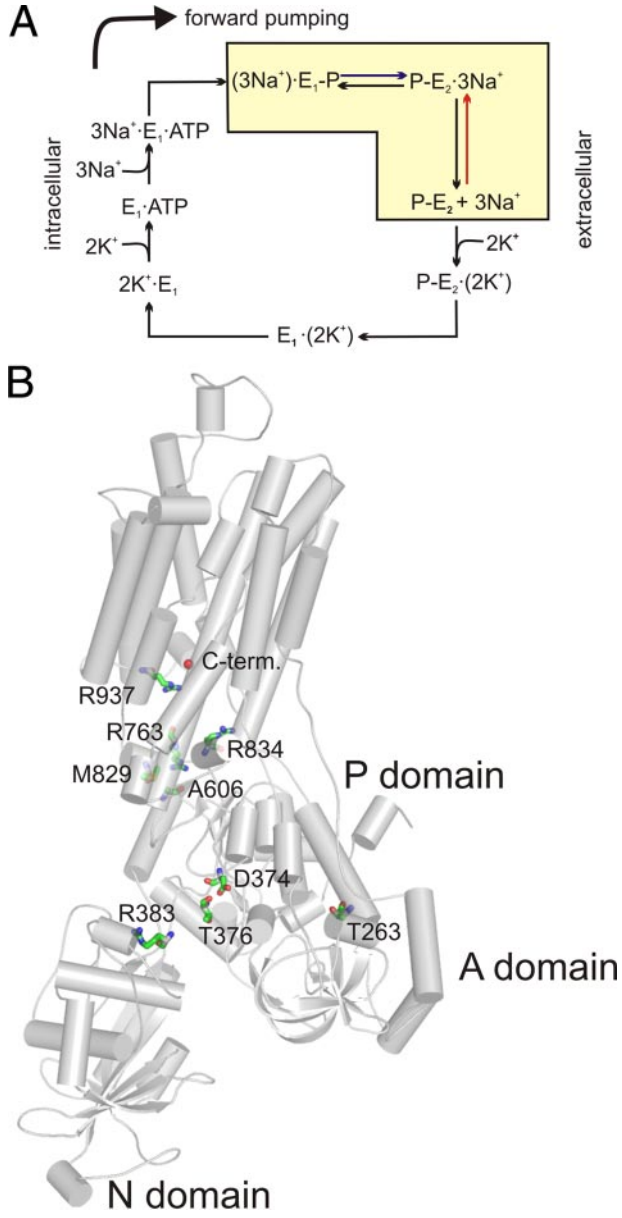

FIGURE 1. **Mechanism and structure of the Na^+/K^+-ATPase.** *A*, reaction cycle of the Na^+/K^+-ATPase. *Yellow*, reaction sequence studied by voltage pulses under high Na^+/K^+-free conditions. *Red arrow*, voltage-dependent reverse binding of extracellular Na^+. *Blue arrow*, conformational change E_1P-E_2P, which is rate-limiting for the forward reaction. *B*, structure of the Na^+/K^+-ATPase according to Protein Data Bank structure entry 3B8E with amino acids numbered according to human ATP1A2. Arg^{763} resides within the M5 helix, Thr^{263} resides in the A domain, Thr^{376} is two residues downstream the phosphorylation site Asp^{374}, and Arg^{383} localizes to one of two "hinge" loops, which link the P and the N domains. Ala^{606} is located at the tip of a short loop between an α-helix and a β-sheet in the P domain, close to Arg^{763} and Met^{829} in the L67 loop (see Fig. 6 for structural details). L67 also contains Arg^{834}. Arg^{937} resides in the M8-M9 loop. *X*1021R generates an extension of the C terminus (*red ball*) by 28 amino acids (RPHWKKNQAWKDGELWRCCGDG-DGEGWK), which is not depicted here.

mutations are located in highly conserved regions that are either core motifs of all P-type ATPases or conserved among all P_2-type ATPases (31). The mutations were selected because of their location in distinct regions within the three-dimensional structure (Fig. 1*B*); T263M is one of three FHM2 mutations in the actuator (A) domain of the enzyme. T376M affects the core sequence SDK**T**GT and is two amino acids apart from Asp^{374}, which forms a phosphorylated intermediate during the reaction cycle. R383H alters a residue within a hinge region between the nucleotide-binding (N) and the phosphorylation (P) domains. The remaining point mutations and del(K935-S940)ins(I) localize to a region, which is critical for interdomain interactions during the catalytic cycle and might also interfere with intracellular access of cations to their binding sites. The Ser^{966} frameshift mutation adds 32 amino acids to the C-terminal end of helix M9 and therefore most likely disrupts helix M10. The *X*1021R mutation results in the addition of 28 amino acids to the C terminus of the enzyme, which according to the recently published crystal structure of the Na^+/K^+-ATPase represents an important regulatory element to optimize Na^+ binding at a putative third binding site (32).

To assess the function of the various *ATP1A2* alleles, we used the two-electrode voltage-clamp technique to analyze stationary and pre-steady state currents and measured Rb^+ uptake and plasma membrane expression in *Xenopus* oocytes. Our findings reveal a broad spectrum of abnormalities, frequently involving changes in the voltage-dependent properties of the enzyme. Mutations that disrupt critical interdomain H-bond patterns, although at distance from the cation-binding pocket, exhibited long range consequences on cation affinities. The expansion of the C terminus of the enzyme by the *X*1021R mutation had a dramatic effect on the interaction with Na^+, supporting the critical role of this highly conserved structural element in voltage sensing and Na^+ transport properties.

EXPERIMENTAL PROCEDURES

cDNA Constructs—Human Na^+/K^+-ATPase α_2- and β_1-subunit cDNAs were subcloned into a modified pCDNA3.1 vector, as described (28). Site-directed mutagenesis was carried out by recombinant PCR. All PCR-derived fragments were verified by sequencing (Eurofins MWG Operon, Ebersberg, Germany). To distinguish the activity of the expressed from the endogenous Na^+/K^+-ATPase, mutations Q116R and N127D were introduced to obtain an ouabain-resistant protein (IC_{50} in millimolar range) (33). The ouabain-resistant wild type α_2-subunit is referred to as WT, and the respective mutants are labeled by their amino acid substitutions, *e.g.* R383H. Nucleotide sequences and nomenclature correspond to those reported in Refs. 5, 17, and 34).

cRNA Synthesis and Oocyte Treatment— cRNA synthesis was carried out with the T7 mMessage mMachine kit (Ambion, Austin, TX). The oocytes were obtained by partial ovarectomy from anesthetized *Xenopus laevis* females, followed by treatment with collagenase 1A (Sigma). Each oocyte was injected with 25 ng of α_2-subunit and 2.5 ng of β_1-subunit cRNAs and stored in ORI buffer (110 mM NaCl, 5 mM KCl, 1 mM $MgCl_2$, 2 mM $CaCl_2$, 5 mM HEPES, pH 7.4) containing 50 mg/liter gentamycin at 18 °C for 3–4 days. Preceding the experiments, intracellular [Na^+] was elevated by 45 min of incubation in Na^+ loading solution (110 mM NaCl, 2.5 mM sodium citrate, 5 mM MOPS, 5 mM Tris, pH 7.4) followed by an incubation of at least 30 min in Na buffer (100 mM NaCl, 1 mM $CaCl_2$, 5 mM $BaCl_2$, 5 mM $NiCl_2$, and 2.5 mM MOPS, 2.5 mM Tris, pH 7.4).

Electrophysiology—Currents were recorded using a Turbotec 10CX amplifier (NPI Instruments, Tamm, Germany) and pClamp 7 software (Axon Instruments, Union City, CA) at room temperature (21–23 °C). The solutions used were: Na buffer (see above), K buffer (100 mM KCl, 5 mM $BaCl_2$, 5 mM $NiCl_2$, 1 mM $CaCl_2$, 2.5 mM MOPS, 2.5 mM Tris, pH 7.4). Sodium-rich buffers containing distinct K^+ concentrations were prepared by mixing appropriate amounts of Na buffer and K buffer (resulting in $(100 - x)$ mM $[Na^+]$ and x mM $[K^+]$, where x is a number between 0 and 10). The $[K^+]_{ext}$-dependent currents were calculated by subtracting currents measured in K^+-free Na buffer from the currents measured in presence of a distinct K^+ concentration. Current amplitudes were corrected for rundown, if necessary. All of the buffers contained 10 μM ouabain to inhibit the endogenous Na^+/K^+-ATPase.

To determine the voltage dependence of stationary currents, the cells were subjected to voltage pulses. Starting from −30-mV holding potential, the cells were clamped to test potentials between −180 and +60 mV (in +20-mV increments), followed by a step back to −30 mV. This protocol was applied first (*a*) in Na buffer, then (*b*) during perfusion with Na-based buffers containing certain $[K^+]$, and (*c*) after washout in Na buffer again. If currents measured during periods *a* and *c* did not differ, the stationary currents were calculated from the difference between corresponding currents measured in periods *b* and *c*. All of the currents within one experiment were normalized to the amplitude at 10 mM K^+ and 0 mV. Voltage-dependent $K_{0.5}$ values for the stimulation of stationary pump currents by extracellular K^+ were determined using fits of the following Hill equation,

$$I = \frac{I_{max}}{1 + \left(\frac{K_{0.5}}{[K^+]}\right)^{n_H}} \quad \text{(Eq. 1)}$$

to the normalized currents at a given membrane potential ($K_{0.5}$ is the concentration of half-maximal activity, and n_H is the Hill coefficient). The Hill parameters from the fits were between 1 and 1.5.

Analysis of Transient Currents—The major electrogenic event within the catalytic cycle is the extracellular release or reverse binding of Na^+. At high Na^+ and extracellularly K^+-free conditions, dephosphorylation is slow, and the enzyme is limited to carrying out electrogenic Na^+/Na^+ exchange (35). Voltage pulses can then shift the enzyme between E_1P and E_2P states (Fig. 1*A*), resulting in transient currents, which yield kinetic information about extracellular Na^+ binding/release and the voltage dependence of the distribution between E_1P and E_2P states. Pre-steady state currents under Na^+/Na^+ exchange conditions were measured as the difference between currents measured first in Na buffer and then in Na buffer containing 10 mM ouabain. The data were fitted monoexponentially disregarding the first 3–5 ms to exclude capacitive artifacts. The charge Q transported during a transient current was determined as the integral of fitted currents, extrapolated to the time of onset of voltage pulses. The resulting Q-V curves were fitted with a Boltzmann function,

$$Q(V) = Q_{min} + \frac{Q_{max} - Q_{min}}{1 + \exp\left(\frac{z_q \cdot F(V - V_{0.5})}{RT}\right)} \quad \text{(Eq. 2)}$$

where Q_{max} and Q_{min} are the saturation values of $Q(V)$, $V_{0.5}$ is the half-maximal voltage, z_q is the fractional charge, F is the Faraday constant, R is the molar gas constant, T is the temperature, and V is the transmembrane potential. A positively shifted $V_{0.5}$ value of a mutant compared with WT is indicative of an increased apparent affinity for extracellular Na^+, because less negative potentials are needed to drive Na^+ movement in conjunction with the E_2P-E_1P conformational change. An equivalent interpretation is an apparent stabilization of the E_1P (or destabilization of the E_2P) conformational state.

Turnover Numbers—The turnover number was calculated by dividing the stationary current (at 10 mM K^+ and −30 mV) by the total moved charge $Q_{tot} = Q_{max} - Q_{min}$ (from fits of Q-V curves with a Boltzmann function), both measured on the same oocyte. For the ATP1A2 WT-expressing cell in Fig. 4*D*, the stationary current and Q_{tot} were 286 nA and 22.6 nC, respectively, resulting in a turnover of 12.7 s^{-1}.

Rb^+ Uptake Measurements—Uptake of Rb^+ into oocytes was measured by atomic absorption spectroscopy using an AAnalyst™ 800 spectrometer (PerkinElmer Life Sciences) equipped with a Rubidium hollow cathode lamp (Photron, Melbourne, Australia) and a transversely heated graphite furnace. After Na^+ loading, the oocytes were incubated for 3 min at 21–22 °C in Na buffer + 1 mM RbCl containing either 10 μM or 10 mM ouabain. After three washes in Rb^+-free Na buffer and one in distilled H_2O, individual cells were homogenized in 1 ml of distilled H_2O. From these homogenates, 20-μl samples were injected into the graphite furnace for analysis.

Isolation of Membrane Fractions from Oocytes—Plasma membranes were prepared as described (36), with some modifications; 8–12 oocytes were rotated for 30 min at 4 °C in Eppendorf cups filled with MBSS buffer (20 mM MES, 80 mM NaCl, pH 6.0) + 1% colloidal silica (Ludox Cl, Sigma), followed by two washes with MBSS. Subsequently, the cells were rotated for 30 min at 4 °C in MBSS + 0.1% polyacrylic acid (Sigma) and then washed twice with MBS buffer (88 mM NaCl, 1 mM KCl, 2.4 mM $NaHCO_3$, 10 mM HEPES, 0.82 mM $MgSO_4$, 0.33 mM $Ca(NO_3)_2$, 0.41 mM $CaCl_2$, pH 7.4). After careful removal of MBS, the oocytes were homogenized in 1500 μl of HbA solution (20 mM Tris, 5 mM $MgCl_2$, 5 mM NaH_2PO_4, 1 mM EDTA, 80 mM sucrose, pH 7.4) containing Complete® protease inhibitor (Roche Applied Science) and centrifuged for 30 s at 10 × *g* (4 °C). The top 1300 μl of these samples, which contained total cellular membranes, were removed and subjected to a total membrane preparation (see below). With the remaining 200 μl, which contained the silica beads with bound plasma membranes, the addition of 1000 μl of HbA, centrifugation, and removal of supernatant were repeated three times (at 10 × *g*, 20 × *g*, and 40 × *g*). After the last low speed centrifugation, plasma membranes were pelleted by centrifugation for 30 min at 16,000 × *g* (4 °C).

For the isolation of total membranes, the supernatant from the first centrifugation step (see previous paragraph) was centrifuged for 3 min at 2,000 × *g* and 4 °C to remove yolk platelets.

Subsequently, the membranes were isolated by centrifugation for 30 min at 16,000 × *g* (4 °C).

All of the samples were solubilized in SDS-PAGE sample buffer (4 μl/oocyte). The aliquots corresponding to the content of one or two oocytes were separated by 10% SDS-PAGE and blotted on polyvinylidene difluoride membranes (Milipore, Bedford, MA). The α_2-subunits of Na^+/K^+-ATPase were detected with the specific polyclonal antibody AB9094 (Chemicon, Temecula, CA).

Structural Examinations and Figures—The analyses of possible H-bonding patterns of the Na^+/K^+-ATPase (Protein Data Bank structure entry 3B8E) and Ca^{2+}-ATPase SERCA ($E_1(Ca^{2+})$ Protein Data Bank structure entry 1SU4 (37) and E_2(TG) Protein Data Bank structure entry 1IWO (38)) were carried out with Swiss Protein Data Bank viewer 3.7. The figures were prepared with PyMOL 1.0r1. Figure presentation and statistical analyses (Student's *t* test) were carried out with Origin 7.5 (OriginLab Corp., Northampton, MA).

RESULTS

Expression in Xenopus Oocytes, K^+-stimulated Pump Currents and Rb^+ Uptake—To assess the ion transport capacity of the various ATP1A2 alleles, Na^+/K^+ pump currents were measured upon stimulation by different extracellular $[K^+]$. Fig. 2*A* shows that the mean pump currents, measured at −30 mV, were significantly reduced compared with WT (all $p > 0.005$). R383H, A606T, R763H, M829R, R834Q, and *X*1021R exhibited mean currents between 27 and 67%. The remaining mutations (T263M, T376M, R937P, del(K935-S940)ins(I), and S966fs) showed either no or very small currents. To assess residual ion pumping activity more sensitively, we determined ouabain-sensitive Rb^+ uptake into individual oocytes using atomic absorption spectrometry. Again, T376M and del(K935-S940)ins(I) showed no significant Rb^+ uptake ($p > 0.05$ compared with uninjected oocytes), and values for T263M, R937P, and S966fs were below 20% of WT (Fig. 2*B*), confirming drastically reduced ion pumping activity. In contrast, *X*1021R showed Rb^+ uptake of ~75% of WT (at 1 mM Rb^+), probably because of its higher K^+ affinity (see below).

To investigate whether the differences in transport activity were due to different expression levels or plasma membrane targeting, we carried out Western blots of simultaneously prepared plasma membrane and total membrane protein fractions. As shown in Fig. 2*C* total protein expression of mutant alleles was not different from WT, which also suggests intact α-β subunit interactions during protein folding and membrane insertion (39). However, analysis of plasma membrane fractions revealed strongly reduced levels of mutants S966fs and del(K935-S940)ins(I) (Fig. 2*C*), indicating that impaired targeting to the cell surface accounts for the absence of pump currents in oocytes expressing these mutants.

Dependence of Stationary Pump Currents on Membrane Potential and $[K^+]_{ext}$—We next determined the $K_{0.5}$ values for extracellular K^+ for mutants that showed sufficiently high pump currents at −30 mV (Table 1). Apparent K^+ affinities were increased for R763H and *X*1021R but decreased for A606T ($p > 0.05$). Examination of the voltage dependence of pump currents revealed altered $[K^+]$-dependent *I-V* curves for

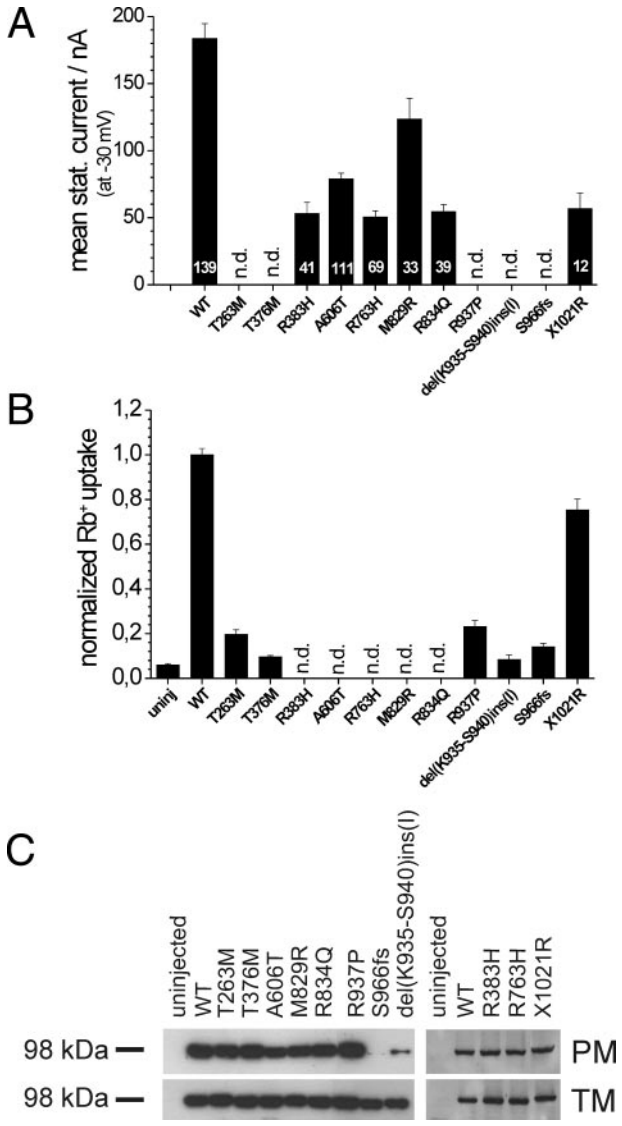

FIGURE 2. **Activity and expression of ATP1A2 constructs.** *A*, mean stationary currents at 10 mM K^+ and −30 mV from oocytes expressing WT and mutant *ATP1A2* alleles. This method could only be applied for the determination of pumping activity for mutants, which consistently yielded currents larger than 10 nA, in other cases (marked *n.d.*) currents in response to 10 mM K^+ did not exceed background current fluctuations. The data were obtained from more than 30 oocyte batches (means ± S.E., numbers of cells are indicated). *B*, residual ion transport activity as assessed by ouabain-sensitive Rb^+ uptake, which was measured as the difference between mean uptake values measured in presence of 10 μM and 10 mM ouabain, respectively, from four batches of cells (n = 14–30 cells; *n.d.*, not determined). Uninjected oocytes served as controls. The data were normalized to WT ATP1A2 measured at 10 μM ouabain (Experiment 1, 49 pmol/oocyte/min; Experiment 2, 130 pmol/oocyte/min; Experiment 3, 38 pmol/oocyte/min; Experiment 4, 61 pmol/oocyte/min). *C*, representative Western blots of protein samples from plasma membrane (*PM*) and total membrane (*TM*) preparations of oocytes expressing various ATP1A2 constructs. The equivalent of one (*left panels*) or two (*right panels*) oocytes was loaded per lane. Uninjected oocytes served as controls. The experiments were repeated three times, with identical results.

A606T, R763H, and R834Q compared with WT (Fig. 3), and the voltage dependence of $K_{0.5}$ values for A606T and R763H was markedly changed (Fig. 3, *insets*). At 10 mM $[K^+]_{ext}$, stationary currents of WT ATP1A2 were in saturation, and the corresponding *I-V* curve increased steadily with voltage (Fig. 3*A*). At $[K^+]_{ext} < 5$ mM, however, bell-shaped *I-V* curves were obtained with a maximum at +20 mV. At subsaturating $[K^+]_{ext}$ the elec-

TABLE 1

$K_{0.5}$ values from $[K^+]_{ext}$ dependence of pump currents and parameters of Boltzmann fits to Q-V curves derived from transient currents (means ± S.E., n = number of cells)

NA, not applicable.

	From stationary pump currents at −30 mV		From transient currents at $[Na^+]_{ext}$ = 100 mM and $[K^+]_{ext}$ = 0		Turnover	n
	$K_{0.5}$ (K^+)	n	$V_{0.5}$	z_q		
	mM		*mV*		s^{-1}	
WT	0.95 ± 0.05	18	4.3 ± 3.5	0.82 ± 0.03	12.8 ± 3.0	18
T263M	NA	NA	NA	NA	NA	NA
T376M	NA	NA	NA	NA	NA	NA
R383H	0.98 ± 0.06	14	30.4 ± 6.4	0.80 ± 0.07	6.1 ± 1.2	12
A606T	1.42 ± 0.12	32	43.2 ± 8.6	0.85 ± 0.07	8.9 ± 2.5	15
R763H	0.72 ± 0.05	25	6.2 ± 6.9	0.81 ± 0.02	4.2 ± 1.8	18
M829R	0.85 ± 0.02	16	−12.0 ± 6.4	0.77 ± 0.04	11.6 ± 3.7	15
R834Q	0.87 ± 0.06	10	25.6 ± 8.6	0.93 ± 0.2	3.6 ± 1.0	6
R937P	NA	NA	NA	NA	NA	NA
S966fs	NA	NA	NA	NA	NA	NA
del(K935-S940)ins(I)	NA	NA	NA	NA	NA	NA
X1021R	0.37 ± 0.05	9	−30 ± 20	0.29 ± 0.03	3.5 ± 1.2	11

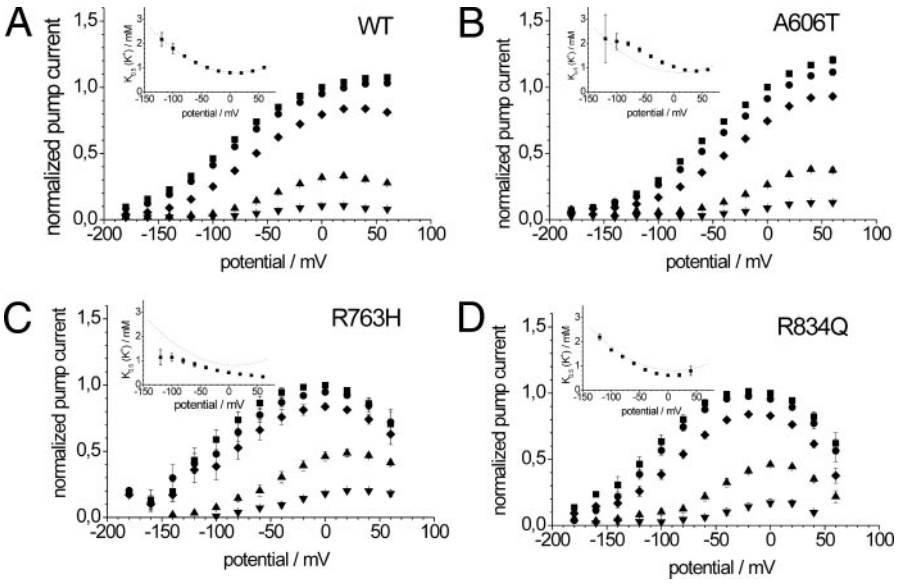

FIGURE 3. **$[K^+]_{ext}$-dependent *I-V* curves and apparent K^+ affinities.** $[K^+]_{ext}$ and voltage dependence of pump currents for ATP1A2 WT (*A*), A606T (*B*), R763H (*C*), and R834Q (*D*). Pump currents were measured in response to voltage steps upon addition of different $[K^+]_{ext}$, and amplitudes at $[K^+]$ = 10 mM and 0 mV were used for normalization. The symbols indicate different $[K^+]$ values: ▼, 0.2 mM; ▲, 0.5 mM; ◆, 2 mM; ●, 5 mM; ■, 10 mM. The values are the means ± S.E. (number of cells/batches: 20/6 for WT, 20/10 for A606T, 5/3 for R763H, 6/3 for R834Q). *Insets*, voltage-dependent $K_{0.5}$ values were determined from fits of a Hill function to the data (WT curve superimposed as *dotted line* for comparison).

trogenic binding of extracellular K^+ is responsible for the decrease of the stationary currents at positive potentials (40). For A606T the maxima of the corresponding *I-V* curves were shifted to +50 mV, and bell-shaped curves were only obtained at $[K^+]_{ext} < 2$ mM (Fig. 3*B*). In contrast, for R763H and R834Q bell-shaped *I-V* curves were even found at saturating extracellular $[K^+]$ (Fig. 3, *C* and *D*), indicating an abnormal decrease of enzyme turnover at positive potentials.

Voltage-dependent $K_{0.5}$ values of WT ATP1A2 (*inset* in Fig. 3*A*) follow a characteristic U-shaped curve with a minimum at 0 mV. The $K_{0.5}$ curve for A606T was positively shifted with a minimum at +50 mV, resulting in increased $K_{0.5}$ values below 0 mV compared with WT. In contrast, $K_{0.5}$ values for R763H were significantly reduced at all potentials, and those of R834Q were slightly smaller than for WT between +20 and −40 mV. Other mutants did not differ from WT in this set of experiments (data not shown). Because of elevated background conductances and current drifts in oocytes expressing *X*1021R, sufficiently stable recordings for repetitive voltage pulse experiments were not feasible.

Kinetics and Voltage Dependence of Transient Currents—To further investigate the properties of electrogenic Na^+ transport, we performed voltage pulse experiments under extracellularly high $[Na^+]$, K^+-free conditions. Fig. 4*B* shows representative ouabain-sensitive transient currents from an oocyte expressing WT ATP1A2. The apparent rate constants were ~80 s^{-1} at positive potentials and exhibited a characteristic increase at negative potentials (Fig. 4*B*). Fig. 4*D* shows the voltage-dependent distribution of translocated charge (*Q-V* curve) for the WT ATP1A2-expressing cell from Fig. 4*B*.

The mean values for the fractional charge z_q and the midpoint potential $V_{0.5}$ from Boltzmann fits of *Q-V* curves for the different ATP1A2 mutants are listed in Table 1. The C-terminal missense mutation *X*1021R led to most striking abnormalities in the behavior of transient currents under electrogenic Na^+/Na^+ exchange conditions. Contrasting with WT (Fig. 4, *B* and *C*), mutant *X*1021R showed an increase of apparent rate constants with positive potentials (Fig. 4, *E* and *F*). Moreover, in all *X*1021R-expressing cells the *Q-V* distribution was nearly linear over the range of potentials investigated (Fig. 4*G*). Thus, the saturation values Q_{max} and Q_{min} from fits of a Boltzmann function were not well defined, and the strongly reduced z_q value of ~0.3, which was consistently derived from the data, likely represents only an upper limit. Therefore, the voltage dependence of charge movement is very shallow compared with WT, implying that electrogenic Na^+ translocation is severely altered for *X*1021R.

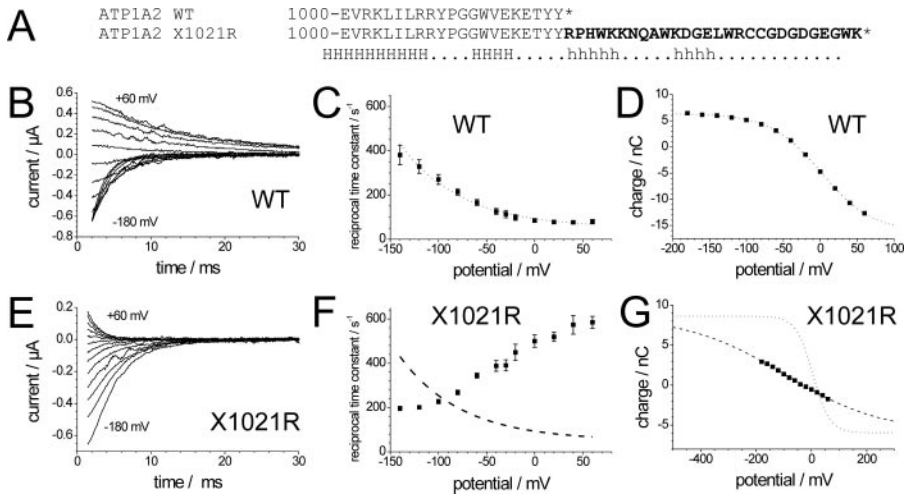

FIGURE 4. **Mutant *X*1021R: Voltage dependence of transient currents under high Na^+/K^+-free conditions.** *A*, C-terminal sequence of ATP1A2 WT and *X*1021R, with the insertion caused by the *X*1021R mutation in *bold letters*. Secondary structure prediction algorithms (*e.g.* PROF in the PredictProtein analysis package) indicate two short α-helical stretches in the extended C terminus (*lowercase h*), α-helices from Protein Data Bank entry 3B8E are indicated by *uppercase H*. *B* and *E*, representative transient currents in response to voltage pulses from −30 mV to potentials between +60 mV and −180 mV (in −20 mV decrements) are shown for WT (*B*) and *X*1021R (*E*). The voltage dependence of reciprocal time constants of transient currents is shown in *C* and *F* with the WT curve (fit of a polynomial function) depicted as *dashed lines*. The data were obtained from 18 (WT) or 12 (*X*1021R) oocytes from at least three frogs (means ± S.E.). *Q-V* curves from integration of transient currents from *B* and *E* are depicted in *D* and *G*, respectively. The values from fits of a Boltzmann function to the data in *D* were: $Q_{max} = 6.38 \pm 0.06$ nC, $Q_{min} = -16.22 \pm 0.30$ nC, $V_{0.5} = 1.5 \pm 1.1$ mV, $z_q = 0.73 \pm 0.02$, and those for data in *G* were, $Q_{max} = 8.6 \pm 1.4$ nC, $Q_{min} = -6.0 \pm 1.6$ nC, $V_{0.5} = -41 \pm 20$ mV, $z_q = 0.29 \pm 0.09$.

The remaining constructs showed z_q values similar to WT. However, various mutants exhibited de- or hyperpolarizingly shifted $V_{0.5}$ values (Table 1 and Fig. 5), indicating changed apparent Na^+ affinities. Apparent rate constants from transient currents for R383H were generally slower than WT values (Fig. 5*A*) and saturated at ~250 s^{-1} at potentials below −120 mV, indicating impaired flexibility during the E_1P to E_2P conformational transition. In contrast, significantly increased rate constants were found for A606T, R763H, M829R, and R834Q (Fig. 5, *C*, *E*, *G*, and *J*). The voltage dependence of rate constants for A606T (Fig. 5*C*) exhibited a shift to depolarizing potentials compared with WT, whereas the values for R763H (Fig. 5*E*), M829R (Fig. 5*G*), and R834Q (Fig. 5*J*) were elevated over the whole range of potentials tested, which emerges as a general feature for the group of mutations within the contact region between helix M5, the P domain, and the L67 loop.

Turnover Numbers—As listed in Table 1, R383H, R763H, and R834Q exhibited significantly reduced turnover numbers ($p > 0.005$) compared with WT, and also the A606T value was slightly smaller. A strongly reduced transport capacity was also found for *X*1021R. Here again, the obtained value (3.5 s^{-1}) only represents an upper limit, because smaller values would result if the linear progression of the *Q-V* curve would extend over a larger voltage range.

DISCUSSION

This study provides a detailed electrophysiological and biochemical characterization of a comprehensive subset of *ATP1A2* alleles implicated in FHM and SHM (17, 34). A broad range of functional abnormalities was observed that can be subdivided into two classes. The first group of mutations is characterized by a severe reduction or loss of catalytic activity or by an impairment of plasma membrane delivery. For these mutations rather straightforward interpretations regarding the underlying structural disruptions can be given. The second group of mutants exhibits more subtle functional impairments, such as changes in apparent cation affinities, voltage dependence, or kinetics, which frequently occur in parallel to a reduction in turnover numbers. These mutations are in the C terminus (*X*1021R) or in regions involved in important interdomain interactions (31, 32). We will discuss this latter group in more detail regarding the relationship between structural and functional disruptions. Of note, all mutant alleles impaired the ability of *ATP1A2* alleles to sustain cell viability in ouabain survival assays, suggesting a loss-of-function effect also on a cellular level (data not shown), in agreement with earlier studies (5, 28, 30).

Mutations Affecting Catalytic Activity or Plasma Membrane Expression—Pump currents and Rb^+ uptake were very small or completely abolished for mutants T263M, T376M, R937P, del(K935-S940)ins(I), and S966fs (Fig. 2). Because the amount of total and plasma membrane protein was normal for T263M, T376M, and R937P, the most likely explanation for the observed loss of function is a decreased or abolished catalytic turnover. For del(K935-S940)ins(I) and S966fs, a severe reduction of plasma membrane protein compared with WT was found (Fig. 2*C*). The Ser^{966} frameshift mutation disrupts the C-terminal sequence of the enzyme starting from the extracellular end of helix M9. Although this is the first time that reduced plasma membrane trafficking or protein stability was found in conjunction with FHM2 mutations, it is evident that a deletion or a frameshift mutation may result in premature degradation caused by improper protein folding and by interference with cellular quality control mechanisms.

A rather obvious explanation can also be provided for mutation T376M. Because Thr^{376} resides in the signature sequence SDK**T**GT and is involved in Mg^{2+} coordination at the catalytic site, the T376M mutant represents a completely dysfunctional enzyme. R937P, like del(K935-S940)ins(I), affects the loop between transmembrane segments M8 and M9. Despite normal protein levels, ion pumping activity was very small for R937P (Fig. 2, *B* and *C*). In the crystal structure of the Na^+/K^+-ATPase (32), Arg^{937} has been implicated in correct positioning of the C terminus of the enzyme by forming H-bonds to Tyr^{1019} and one of the terminal oxygen atoms of the C terminus (Fig. 6*A*). The latter is further stabilized against M5 by H-bonds of Tyr^{1020} and the other C-terminal oxygen with Lys^{770}. This arrangement was suggested to be important for correct formation of a putative third Na^+-binding site (32). Furthermore, it

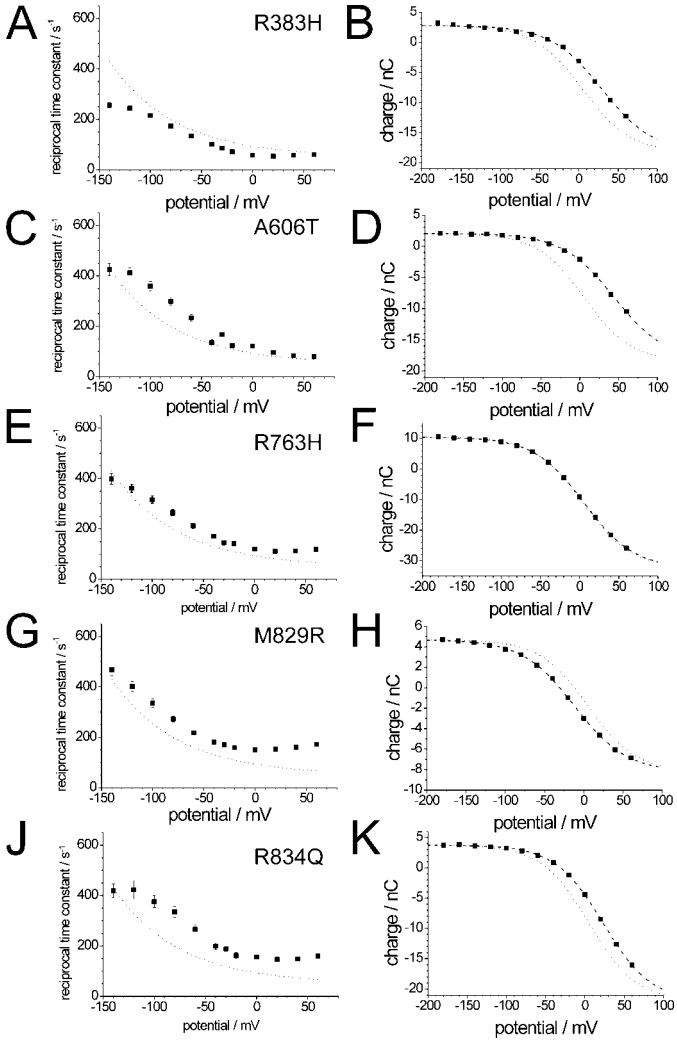

FIGURE 5. **Reciprocal time constants and *Q-V* curves.** The *left panels* show reciprocal time constants (means ± S.E.) from transient currents measured under high Na^+/K^+-free conditions for R383H ($n = 12$) (*A*), A606T ($n = 19$) (*C*), R763H ($n = 18$) (*E*), M829R ($n = 15$) (*G*), and R834Q ($n = 6$) (*J*). The *right panels* depict *Q-V* curves from single representative cells expressing these constructs. The *dashed lines* resulted from fits of a Boltzmann function to the *Q-V* curves, with parameters as follows: *B*, $Q_{max} = 2.8 \pm 0.2$ nC, $Q_{min} = -18.3 \pm 1.9$ nC, $V_{0.5} = 29.2 \pm 6.6$ mV, $z_q = 0.76 \pm 0.07$; *D*, $Q_{max} = 2.05 \pm 0.07$ nC, $Q_{min} = -18.5 \pm 1.5$ nC, $V_{0.5} = 44.4 \pm 5.1$ mV, $z_q = 0.75 \pm 0.04$; *F*, $Q_{max} = 10.43 \pm 0.07$ nC, $Q_{min} = -32.4 \pm 0.4$ nC, $V_{0.5} = 5.6 \pm 0.7$ mV, $z_q = 0.80 \pm 0.01$; *H*, $Q_{max} = 4.69 \pm 0.05$ nC, $Q_{min} = -8.2 \pm 0.2$ nC, $V_{0.5} = -12.1 \pm 1.1$ mV, $z_q = 0.76 \pm 0.02$; *K*, $Q_{max} = 3.74 \pm 0.05$ nC, $Q_{min} = -22.0 \pm 0.5$ nC, $V_{0.5} = 23.4 \pm 1.3$ mV, $z_q = 0.83 \pm 0.02$. In both cases an appropriately scaled *Q-V* curve of the WT-expressing cell from Fig. 4*C* is superimposed (*dotted line*).

was proposed that Arg^{937} is part of a C-terminal cluster of arginines, which might be involved in voltage sensitivity, similar to the voltage sensor arginines in voltage-gated cation channels (32). Because replacement of Arg^{937} by proline can cause backbone distortions and disrupt H-bond patterns, positioning of the Na^+/K^+-ATPase C terminus is possibly disturbed. Thus, the M8-M9 loop appears to be critical in preserving the native enzyme structure and in coordinated interdomain interactions during the catalytic cycle.

Somewhat more subtle are the consequences of the T263M mutation, which is one of three FHM mutations identified in the A domain so far and affects a conserved residue within the third core motif of P-type ATPases (31). Functional consequences were severe, because currents and transport capacity in Rb^+ uptake experiments were reduced to below 10% of WT (Fig. 2). Because plasma membrane expression was normal, the decrease in pumping activity is most likely due to a drastic reduction in turnover. In the Na^+/K^+-ATPase crystal structure (32) Thr^{263} resides in the intracellular M2-M3 loop at the C-terminal end of a short α-helix, at which helix M3 drags to move the A domain during the E_1-E_2 conformational change. Inspection of the crystal structures of the homologous Ca^{2+}-ATPase SERCA reveals that during this conformational transition the α-helical pattern around the corresponding SERCA-Thr^{230} is partially broken (37, 38). If a similar mechanism would apply for the Na^+/K^+-ATPase, the bulkier methionine side chain could sterically disrupt the local structure including the hydrogen bonding pattern around the mutated residue and thus impair the coupling of helix M3 movement to the A domain. The dramatic reduction in activity highlights the critical role of the respective core motif for function of the Na^+/K^+-ATPase.

A similar interpretation can be provided for R383H, which was characterized by a 48% decrease in catalytic turnover. Arg^{383} is highly conserved within the fifth core motif of P-type ATPases and resides in a hinge region (homologous to SERCA-Gln^{360} within the TN**Q**MS loop motif), which flexibly links the N domain to the P domain (Fig. 1*B*). Because the N domain undergoes considerable movements toward the P domain during the catalytic cycle, the R383H mutation apparently interferes with the flexibility during conformational changes. This interpretation is supported by the observed reduction of rate constants during the voltage jump-induced $E_1P \leftrightarrow E_2P$ conformational transition and the reduced turnover number. The additionally observed shift of the *Q-V* curve derived from transient currents by about +26 mV indicates an effect on conformational equilibria, suggesting a relative stabilization of the E_1P conformation at physiological potentials. Of interest, the recently reported FHM mutation R593W (16) localizes to the second hinge between N and P domain. Largely reduced cell survival has been reported for this variant, emphasizing the critical role of these hinges for conformational flexibility and thus pumping rate.

Mutations of Residues Involved in H-bond Networks at the Interface between the L67, P, and TM Domains—A606T, R763H, M829R, and R834Q affect highly conserved residues involved in interdomain H-bond networks of P-type ATPases. Apart from a reduction of the turnover number, which was observed for most mutations, the main findings for this group of mutations involve increased rate constants of transient currents (Fig. 5, *C*, *G*, *E*, and *J*). In addition, subtle changes in other voltage-dependent properties or cation affinities were found. In the Na^+/K^+-ATPase crystal structure (32) the distinct hydrogen bonding networks between Ala^{606}, Arg^{763}, Met^{829}, and Gly^{365} (Fig. 6*B*) stabilize the relative positions of the L67 loop (Met^{829}), the P domain (Ala^{606} and backbone oxygen of Gly^{365}), and helix M5 (Arg^{763}). In addition, Arg^{834} forms H-bonds to Asp^{839} (L67) and Ser^{366} (P domain) (Fig. 6*C*). Such H-bond networks have already been pointed out between SERCA residues Ala^{617}, Arg^{751}, and Met^{817} (37, 38), which correspond to

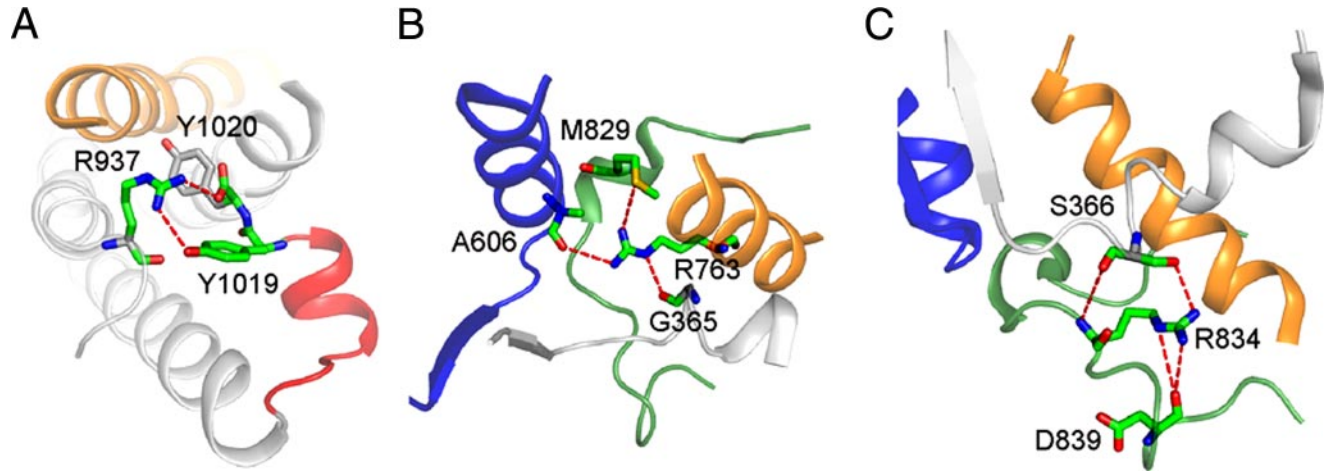

FIGURE 6. **H-bonding patterns.** Shown are the structure details of the interfacial region between P and transmembrane domain and the L67 loop of the Na^+/K^+-ATPase (according to Protein Data Bank entry 3B8E). Amino acids are shown in ball-and-stick representation and numbered according to the human ATP1A2 sequence. H-bonds (*red dashed lines*) with a 3.3 Å cut-off distance are shown. *A*, H-bonds between R937 (M8-M9 loop), Tyr^{1019}, and the C terminus of the Na^+/K^+-ATPase. Tyr^{1021} is also shown, which forms a contact to helix M5 (*orange*). *B*, H-bonds around R763, showing linkage to L67 (Met^{829}) and the P domain (Ala^{606} and backbone carbonyl oxygen of Gly^{365}). *C*, H-bonds of R834 (L67 loop), with Asp^{839} (also in L67) and Ser^{366} (P domain).

ATP1A2 residues Ala^{606}, Arg^{763}, and Met^{829}, respectively. During the conformational change from the SERCA $E_1(Ca^{2+})$ structure (Protein Data Bank entry 1SU4 (37)) to the E_2(TG) structure (Protein Data Bank entry 1IWO (38)), H-bonds are slightly rearranged but stay intact between Arg^{751} and Ala^{617} or Met^{817}, indicating that the local structure needs to be rather rigidly stabilized during catalysis. Further C-terminally, SERCA residue Arg^{822} (corresponding to ATP1A2 Arg^{834}) is hydrogen-bonded via a water molecule to a conserved Glu residue within the first α-helix of the P domain (37). Thus, it is likely that ATP1A2 residues Ala^{606}, Arg^{763}, Met^{829}, and Arg^{834} are critically involved in structural stabilization of this interdomain interface region during the catalytic cycle. It emerges as a general feature that mutations that are expected to disrupt these H-bonding patterns cause an abnormally high flexibility during the E_1P to E_2P conformational transition.

A major finding of this study was that mutations of various residues within a hydrogen-bonded network of amino acids between various enzyme domains do not lead to a complete inactivation of the Na^+ pump but induce changes in the kinetics of the E_1P to E_2P conformational change and of voltage-dependent properties, accompanied by complex long range effects on cation interactions. Because the interdomain interaction region is located at some distance from the cation-binding pocket, the observed changes in cation affinities cannot be explained by structural disruptions within the immediate vicinity of the mutated residues. However, the abnormally increased rate constants of the voltage jump-induced redistribution between E_1P and E_2P states can directly affect the poise of the voltage-dependent distribution between these two states. Indeed, shifted *Q-V* curves were predominantly observed that directly indicate changes of the voltage-dependent distribution between E_1P and E_2P. Therefore, in accordance with previous suggestions by Jørgensen *et al.* (41), it can be argued that the observed changes in the apparent affinities for cations occur secondary to shifts in conformational equilibria. However, the observed long range effects are complex, because shifts in the dynamic E_1P-E_2P equilibrium do not consistently correlate with cation affinity changes: On one hand, for A606T K^+ affinity was decreased, but the *Q-V* curve was shifted to positive potentials, in line with an increased Na^+ affinity or a relative stabilization of the E_1P state. On the other hand, for R763H an increased K^+ affinity was measured, but the *Q-V* curve was not shifted; thus, Na^+ affinity or the poise of the equilibrium between E_1P and E_2P states was not changed. In contrast, mutations M829R and R834Q left the apparent K^+ affinity unchanged, but from the observed shifts of the Q-V curves either a decrease (M829R) or an increase (R834Q) of the apparent affinity for extracellular Na^+ could be inferred. Therefore, the observed affinity changes are most likely due to a complex superposition of, first, direct long range structural effects on the configuration of cation coordinating residues and, second, changes in kinetics that induce shifts in conformational equilibria. The consistently observed elevation of the apparent rate constants from transient currents for mutants A606T, R763H, M829R, and R834Q indicates an abnormally high flexibility during the E_1P-E_2P conformational change, in line with a destabilizing effect of the respective mutations. Although all these changes can explain impairment of Na^+/K^+-ATPase function under physiological conditions, it will be challenging to consistently reconcile the observed functional abnormalities with structural considerations or predictions from structural modeling.

*Expansion of the C Terminus by Mutation X*1021R—In accordance with the suggestions of Morth *et al.* (32), who proposed a significant influence of the Na^+/K^+-ATPase C terminus on voltage sensitivity and cation coordination, several striking functional abnormalities were observed for this mutant. A strong increase in the apparent affinity for extracellular K^+ was determined, paralleled by a decreased apparent affinity for Na^+, as derived from the negatively shifted *Q-V* curve. In addition, the turnover number was reduced by 70% compared with WT. The relatively high Rb^+ uptake (~75% of WT), which was measured at 1 mM [Rb^+], can be explained by the increased K^+ affinity of *X*1021R, so that the transport rate for the mutant construct is close to saturation, whereas turnover is only about

half-maximal for the WT enzyme under these conditions. Furthermore, voltage dependence and kinetics of transient currents were completely different from WT, because the apparent rate constants increased with positive potentials. Such an inverted behavior has only been described for a mutation (D808E) that explicitly affects one of the cation-coordinating residues within the Na^+/K^+-ATPase cation-binding pocket (39, 42). To account for such a voltage dependence of rate constants, one of the reaction steps within Na^+ forward transport (*i.e.* Na^+ binding from intracellular, E_1P-E_2P conformational change, or extracellular Na^+ release) must be voltage-dependent for *X*1021R (43). This is in contrast to WT, in which reverse binding of extracellular Na^+ underlies voltage dependence (Fig. 1*A*). Also in contrast to WT, the voltage dependence of charge movement (z_q from *Q-V* curve) was much weaker and thus electrogenicity of Na^+ transport was drastically reduced. In summary, our data suggest that severe changes in the properties of electrogenic Na^+ transport underlie *X*1021R behavior and support the notion that the C terminus of Na^+/K^+-ATPase critically affects voltage sensitivity and interaction with Na^+. At any rate the observed alterations severely affect the ability of the protein to maintain the physiologically required gradients for Na^+ and K^+.

Functional Defects of ATP1A2 Alleles and Migraine—How can these findings be reconciled with the occurrence of migraine attacks in patients with FHM and SHM? Most of the aura symptoms in migraine are generated by cortical spreading depression (CSD) or CSD-like events that are characterized by a spreading front of excitation (depolarization), followed by long lasting depression (hyperpolarization) (44–47). All of the mutations investigated here resulted in a partial or complete loss of activity of the Na^+/K^+-ATPase, yet because of diverse functional abnormalities. Loss of function of the Na^+/K^+ pump may lead to neuronal (and glial) depolarization through various ways. First, because of the critical role of K^+ channels for repolarization, a reduction of the K^+ gradient might destabilize the membrane resting potential and thus reduce the activation threshold. Second, breakdown of the Na^+ gradient might affect removal of the excitatory neurotransmitter glutamate from the synaptic cleft, which is driven by the astrocytic Na^+/glutamate transporter. Elevated levels of extracellular glutamate have been shown to trigger CSD. Third, impairment of the Na^+ gradient might cause elevated intracellular Ca^{2+}, augmented Ca^{2+} influx into the endoplasmatic reticulum, which in turn leads to increased Ca^{2+} signaling (48). This is because the Na^+ gradient is the energy source for the Na^+/Ca^{2+} exchanger. Together, these changes might contribute to the occurrence of CSD and CSD-like events in patients with FHM and SHM.

Conclusions—Our study identifies reduced or altered activity of the Na^+/K^+-ATPase as the common denominator associated with *ATP1A2* mutations in familial and sporadic hemiplegic migraine. Among the variety of molecular phenotypes, most of the observed changes involve voltage-dependent properties that are critically important for this electrically active enzyme within a physiological context. Our results demonstrate that mutations of residues that are involved in relative stabilization of different enzyme domains during conformational changes result in abnormally high rate constants during the E_1P-E_2P conformational change and evoke intricate long range consequences on cation interactions. The complexity of these long range effects is illustrated by the finding that shifts in the E_1P-E_2P equilibria do not consistently correlate with changes in apparent cation affinities. Furthermore, our observations on *X*1021R strongly support conclusions by Morth *et al.* (32), who outlined the distinct impact of the C terminus on cation coordination, electrogenicity, and voltage dependence of cation transport. This hallmark of the Na^+/K^+-ATPase structure deserves further elucidation by systematic structure-function studies.

Acknowledgments—We thank Renate Gauss (IonGate Biosciences) for donating the human Na^+/K^+-ATPase cDNAs; Verena Pintschovius, Eva Kaindl, and Janna Lustig for excellent technical assistance; and Bas Stunnenberg for help with the ouabain survival assays.

REFERENCES

1. Ophoff, R. A., Terwindt, G. M., Vergouwe, M. N., van Eijk, R., Oefner, P. J., Hoffman, S. M., Lamerdin, J. E., Mohrenweiser, H. W., Bulman, D. E., Ferrari, M., Haan, J., Lindhout, D., van Ommen, G. J., Hofker, M. H., Ferrari, M. D., and Frants, R. R. (1996) *Cell* **87,** 543–552
2. Ducros, A., Denier, C., Joutel, A., Cecillon, M., Lescoat, C., Vahedi, K., Darcel, F., Vicaut, E., Bousser, M. G., and Tournier-Lasserve, E. (2001) *N. Engl. J. Med.* **345,** 17–24
3. Dichgans, M., Freilinger, T., Eckstein, G., Babini, E., Lorenz-Depiereux, B., Biskup, S., Ferrari, M. D., Herzog, J., van den Maagdenberg, A. M., Pusch, M., and Strom, T. M. (2005) *Lancet* **366,** 371–377
4. Vanmolkot, K. R., Babini, E., de Vries, B., Stam, A. H., Freilinger, T., Terwindt, G. M., Norris, L., Haan, J., Frants, R. R., Ramadan, N. M., Ferrari, M. D., Pusch, M., van den Maagdenberg, A. M., and Dichgans, M. (2007) *Hum. Mutat.* **28,** 522
5. De Fusco, M., Marconi, R., Silvestri, L., Atorino, L., Rampoldi, L., Morgante, L., Ballabio, A., Aridon, P., and Casari, G. (2003) *Nat. Genet.* **33,** 192–196
6. Todt, U., Dichgans, M., Jurkat-Rott, K., Heinze, A., Zifarelli, G., Koenderink, J. B., Goebel, I., Zumbroich, V., Stiller, A., Ramirez, A., Friedrich, T., Gobel, H., and Kubisch, C. (2005) *Hum. Mutat.* **26,** 315–321
7. Albers, R. W. (1967) *Ann. Rev. Biochem.* **36,** 727–756
8. Post, R. L., Hegyvary, C., and Kume, S. (1972) *J. Biol. Chem.* **247,** 6530–6540
9. Kaplan, J. H. (2002) *Annu. Rev. Biochem.* **71,** 511–535
10. Jørgensen, P. L., Hakansson, K. O., and Karlish, S. J. (2003) *Annu. Rev. Physiol.* **65,** 817–849
11. Orlowski, J., and Lingrel, J. B. (1988) *J. Biol. Chem.* **263,** 10436–10442
12. McGrail, K., Phillips, J. M., and Sweadner, K. J. (1991) *J. Neurosci.* **11,** 381–391
13. Moseley, A. E., Lieske, S. P., Wetzel, R. K., James, P. F., He, S., Shelly, D. A., Paul, R. J., Boivin, G. P., Witte, D. P., Ramirez, J.-M., Sweadner, K. J., and Lingrel, J. B. (2003) *J. Biol. Chem.* **278,** 5317–5324
14. Peng, L., Martin-Vasallo, P., and Sweadner, K. J. (1997) *J. Neurosci.* **17,** 3488–3502
15. Watts, A. G., Sanchez-Watts, G., Emanuel, J. R., and Levenson, R. (1991) *Proc. Natl. Acad. Sci. U. S. A.* **88,** 7425–7429
16. Vanmolkot, K. R., Kors, E. E., Turk, U., Turkdogan, D., Keyser, A., Broos, L. A., Kia, S. K., van den Heuvel, J. J., Black, D. F., Haan, J., Frants, R. R., Barone, V., Ferrari, M. D., Casari, G., Koenderink, J. B., and van den Maagdenberg, A. M. (2006) *Eur. J. Hum. Genet.* **14,** 555–560
17. Jurkat-Rott, K., Freilinger, T., Dreier, J. P., Herzog, J., Gobel, H., Petzold, G. C., Montagna, P., Gasser, T., Lehmann-Horn, F., and Dichgans, M. (2004) *Neurology* **62,** 1857–1861
18. Kaunisto, M. A., Harno, H., Vanmolkot, K. R., Gargus, J. J., Sun, G., Hamalainen, E., Liukkonen, E., Kallela, M., van den Maagdenberg, A. M., Frants, R. R., Farkkila, M., Palotie, A., and Wessman, M. (2004) *Neuroge-*

netics **5,** 141–146
19. Spadaro, M., Ursu, S., Lehmann-Horn, F., Liana, V., Giovanni, A., Paola, G., Frontali, M., and Jurkat-Rott, K. (2004) *Neurogenetics* **5,** 177–185
20. Vanmolkot, K. R., Kors, E. E., Hottenga, J. J., Terwindt, G. M., Haan, J., Hoefnagels, W. A., Black, D. F., Sandkuijl, L. A., Frants, R. R., Ferrari, M. D., and van den Maagdenberg, A. M. (2003) *Ann. Neurol.* **54,** 360–366
21. Vanmolkot, K. R., van den Maagdenberg, A. M., Haan, J., and Ferrari, M. D. (2003) *Lancet Neurol.* **2,** 721
22. Riant, F., De Fusco, M., Aridon, P., Ducros, A., Ploton, C., Marchelli, F., Maciazek, J., Bousser, M. G., Casari, G., and Tournier-Lasserve, E. (2005) *Hum. Mutat.* **26,** 281–287
23. Swoboda, K. J., Kanavakis, E., Xaidara, A., Johnson, J. E., and Leppert, M. F. (2004) *Ann. Neurol.* **55,** 884–887
24. Vanmolkot, K. R., Stroink, H., Koenderink, J. B., Kors, E. E., van den Heuvel, J. J., van den Boogerd, E. H., Stam, A. H., Haan, J., De Vries, B. B., Terwindt, G. M., Frants, R. R., Ferrari, M. D., and van den Maagdenberg, A. M. (2006) *Ann. Neurol.* **59,** 310–314
25. Pierelli, F., Grieco, G. S., Pauri, F., Pirro, C., Fiermonte, G., Ambrosini, A., Costa, A., Buzzi, M. G., Valoppi, M., Caltagirone, C., Nappi, G., and Santorelli, F. M. (2006) *Cephalalgia* **26,** 324–328
26. Thomsen, L. L., Kirchmann, M., Bjornsson, A., Stefansson, H., Jensen, R. M., Fasquel, A. C., Petursson, H., Stefansson, M., Frigge, M. L., Kong, A., Gulcher, J., Stefansson, K., and Olesen, J. (2007) *Brain* **130,** 346–356
27. Tonelli, A., Gallanti, A., Bersano, A., Cardin, V., Ballabio, E., Airoldi, G., Redaelli, F., Candelise, L., Bresolin, N., and Bassi, M. (2007) *Clin. Genet.* **72,** 517–523
28. Koenderink, J. B., Zifarelli, G., Qiu, L. Y., Schwarz, W., De Pont, J. J., Bamberg, E., and Friedrich, T. (2005) *Biochim. Biophys. Acta* **1669,** 61–68
29. Segall, L., Scanzano, R., Kaunisto, M. A., Wessman, M., Palotie, A., Gargus, J. J., and Blostein, R. (2004) *J. Biol. Chem.* **279,** 43692–43696
30. Segall, L., Mezzetti, A., Scanzano, R., Gargus, J. J., Purisima, E., and Blostein, R. (2005) *Proc. Natl. Acad. Sci. U. S. A.* **102,** 11106–11111
31. Axelsen, K. B., and Palmgren, M. G. (1998) *J. Mol. Evol.* **46,** 84–101
32. Morth, J. P., Pedersen, B. P., Toustrup-Jensen, M. S., Sorensen, T. L., Petersen, J., Andersen, J. P., Vilsen, B., and Nissen, P. (2007) *Nature* **450,** 1043–1049
33. Price, E. M., and Lingrel, J. B. (1988) *Biochemistry* **27,** 8400–8408
34. Riant, F., De Fusco, M., Aridon, P., Ducros, A., Ploton, C., Marchelli, F., Maciazek, J., Bousser, M. G., Casari, G., and Tournier-Lasserve, E. (2005) *Hum. Mutat.* **26,** 281
35. Nakao, M., and Gadsby, D. C. (1986) *Nature* **323,** 628–630
36. Kamsteeg, E. J., and Deen, P. M. (2001) *Biochem. Biophys. Res. Commun.* **282,** 683–690
37. Toyoshima, C., Nakasako, M., Nomura, H., and Ogawa, H. (2000) *Nature* **405,** 647–655
38. Toyoshima, C., and Nomura, H. (2002) *Nature* **418,** 605–611
39. Koenderink, J. B., Geibel, S., Grabsch, E., De Pont, J. J., Bamberg, E., and Friedrich, T. (2003) *J. Biol. Chem.* **278,** 51213–51222
40. Rakowski, R. F., Vasilets, L. A., LaTona, J., and Schwarz, W. (1991) *J. Membr. Biol.* **121,** 177–187
41. Jørgensen, P. L., Jørgensen, J. R., and Pedersen, P. A. (2001) *J. Bioenerg. Biomembr.* **33,** 367–377
42. Ogawa, H., and Toyoshima, C. (2002) *Proc. Natl. Acad. Sci. U. S. A.* **99,** 15977–15982
43. De Weer, P., Rakowski, R. F., and Gadsby, D. C. (1994) in *The Sodium Pump* (Bamberg, E., and Schoner, W., eds) Steinkopff, Darmstadt, 472–481
44. Pietrobon, D., and Striessnig, J. (2003) *Nat. Rev. Neurosci.* **4,** 386–398
45. Moskowitz, M. A., Bolay, H., and Dalkara, T. (2004) *Ann. Neurol.* **55,** 276–280
46. Hadjikhani, N., Sanchez del Rio, M., Wu, O., Schwartz, D., Bakker, D., Fischl, B., Kwong, K. K., Cutrer, F. M., Rosen, B. R., Tootell, R. B. H., Sorensen, A. G., and Moskowitz, M. A. (2001) *Proc. Natl. Acad. Sci. U. S. A.* **98,** 4687–4692
47. Somjen, G. G. (2001) *Physiol. Rev.* **81,** 1065–1096
48. Golovina, V. A., Song, H., James, P. F., Lingrel, J. B., and Blaustein, M. P. (2003) *Am. J. Physiol.* **284,** C475–C486